

# Large-scale, multi-centre, multi-disease validation of an AI clinical tool for cine CMR analysis

## **AUTHORS:**

Jorge Mariscal-Harana, *PhD*,<sup>a</sup>, Clint Asher, *MD*,<sup>a,b</sup>, Vittoria Vergani, *MD*,<sup>a</sup>, Maleeha Rizvi, *MD*,<sup>a,b</sup>, Louise Keehn, *PhD*,<sup>c</sup>, Raymond J. Kim, *MD*,<sup>d</sup>, Robert M. Judd, *PhD*,<sup>d</sup>, Steffen E. Petersen, *MD, PhD*,<sup>e,f,g,h</sup>, Reza Razavi, *MD, PhD*,<sup>a,b</sup>, Andrew King, *PhD*,<sup>a</sup>, Bram Ruijsink, *MD, PhD*,<sup>a,b,i,\*</sup>, Esther Puyol-Antón, *PhD*,<sup>a,\*</sup>

\* Shared last authors

## **AFFILIATIONS:**

- a) School of Biomedical Engineering and Imaging Sciences, King's College London, UK
- b) Department of Adult and Paediatric Cardiology, Guy's and St Thomas' NHS Foundation Trust, London, UK
- c) Cardiovascular Division, Department of Clinical Pharmacology, King's College London British Heart Foundation Centre, St Thomas' Hospital, Westminster Bridge Road, London, UK
- d) Division of Cardiology, Department of Medicine, Duke University, Durham, North Carolina, USA
- e) National Institute for Health Research (NIHR) Barts Biomedical Research Centre, William Harvey Research Institute, Queen Mary University London, London, UK
- f) Barts Heart Centre, St Bartholomew's Hospital, Barts Health NHS Trust, London, UK
- g) Health Data Research UK, London, UK
- h) Alan Turing Institute, London, UK
- i) Department of Cardiology, Heart and Lung Division, University Medical Center Utrecht, Utrecht, The Netherlands

**FUNDING:**

This work was supported by the EPSRC (EP/R005516/1) and the Advancing Impact Award scheme of the Impact Acceleration Account at King's College London. SEP, RR, and AK acknowledge funding from the EPSRC through the SmartHeart Programme grant (EP/P001009/1). JM-H, RR, AK, BR, and EP-A acknowledge support from the Wellcome/EPSRC Centre for Medical Engineering at King's College London (WT 203148/Z/16/Z), the National Institute for Health Research (NIHR) Cardiovascular MedTech Co-operative award to the Guy's and St Thomas' NHS Foundation Trust, and the NIHR comprehensive Biomedical Research Centre award to Guy's & St Thomas' NHS Foundation Trust in partnership with King's College London. SEP acknowledges the British Heart Foundation for funding the manual analysis to create a cardiovascular magnetic resonance imaging reference standard for the UK Biobank imaging resource in 5,000 CMR scans ([www.bhf.org.uk](http://www.bhf.org.uk); PG/14/89/31194). SEP acknowledges support from the NIHR Biomedical Research Centre at Barts. SEP has received funding from the European Union's Horizon 2020 Research and Innovation Programme under grant agreement No 825903 (euCanSHare project). SEP also acknowledges support from the CAP-AI Programme, London's First AI Enabling Programme focused on stimulating growth in the capital's AI Sector. CAP-AI was led by Capital Enterprise in partnership with Barts Health NHS Trust and Digital Catapult and was funded by the European Regional Development Fund and Barts Charity. SEP acknowledges support from the Health Data Research UK, an initiative funded by UK Research and Innovation, the Department of Health and Social Care (England) and the devolved administrations, and leading medical research charities. The views expressed are those of the author(s) and not necessarily those of the EPSRC, the NHS, the NIHR, the Department of Health, or the British Heart Foundation. For the purpose of open access, the author has applied for a CC BY public copyright licence for any Author Accepted Manuscript version arising from this submission. This research has been conducted using the UK Biobank Resource (application 17806). The UK Biobank data are available for approved projects from <https://www.ukbiobank.ac.uk/>.

**RELATIONSHIPS WITH INDUSTRY AND OTHER ENTITIES:**

SEP provided consultancy to Circle Cardiovascular Imaging, Inc., Calgary, Alberta, Canada. RMJ is an employee of Intelrad Medical Systems Inc., Montreal, Canada. The remaining authors declare that the research was conducted without any commercial or financial relationships that could be construed as a potential conflict of interest.

**ADDRESS FOR CORRESPONDENCE:**

Esther Puyol-Antón  
The Rayne Institute  
4th Floor Lambeth Wing, St Thomas Hospital  
Westminster Bridge Road  
SE1 7EH London, United Kingdom  
E-mail: [esther.puyol\\_anton@kcl.ac.uk](mailto:esther.puyol_anton@kcl.ac.uk)

## **STRUCTURED ABSTRACT:**

**Objectives:** To develop and validate a robust CMR analysis tool for automatic segmentation and cardiac function analysis which achieves state-of-the-art performance for multi-centre short-axis cine CMR images.

**Background:** Artificial intelligence (AI) has the potential to facilitate the automation of CMR analysis for biomarker extraction. However, most AI algorithms are trained on a specific input domain (e.g., single scanner vendor or hospital-tailored imaging protocol) and lack the robustness to perform optimally when applied to CMR data from other input domains.

**Methods:** Our proposed framework consists of an AI-based algorithm for biventricular segmentation of short-axis images, followed by a post-analysis quality control to detect erroneous results. The segmentation algorithm was trained on a large dataset of clinical CMR scans from two NHS hospitals (n=2793) and validated on additional cases from this dataset (n=441) and on five external datasets (n=6808). The validation data included CMR scans of patients with a range of diseases acquired at 12 different centres using CMR scanners from all major vendors.

**Results:** Our method yielded median Dice scores over 87%, translating into median absolute errors in cardiac biomarkers within the range of inter-observer variability: <8.4mL (left ventricle), <9.2mL (right ventricle), <13.3g (left ventricular mass), and <5.9% (ejection fraction) across all datasets. Stratification of cases according to phenotypes of cardiac disease and scanner vendors showed good agreement.

**Conclusions:** We show that our proposed tool, which combines a state-of-the-art AI algorithm trained on a large-scale multi-domain CMR dataset with a post-analysis quality control, allows us to robustly deal with routine clinical data from multiple centres, vendors, and cardiac diseases. This is a fundamental step for the clinical translation of AI algorithms. Moreover, our method yields a range of additional biomarkers of cardiac function (filling and ejection rates, regional wall motion, and strain) at no extra computational cost.

## **KEYWORDS:**

Cardiac function, cardiac magnetic resonance, deep learning, quality control, cardiac segmentation, artificial intelligence

## **ABBREVIATIONS AND ACRONYMS:**

AI = artificial intelligence  
CMR = cardiac magnetic resonance  
DL = deep learning  
ED = end-diastole/diastolic  
EDV = end-diastolic volume  
EF = ejection fraction  
ES = end-systole/systolic  
ESV = end-systolic volume  
LV = left ventricle/ventricular  
LVBP = left ventricular blood pool  
LVM = left ventricular mass  
MYO = left ventricular myocardium  
QA = quality assessment  
QC = quality control  
RV = right ventricle/ventricular  
RVBP = right ventricular blood pool

# Introduction

Cardiac Magnetic Resonance (CMR) is the gold standard for biventricular volume and function quantification alongside myocardial tissue characterisation <sup>1</sup>. A wealth of biomarkers for regional and global systolic and diastolic biventricular function can be obtained from short-axis cine CMR, including volumes, ventricular filling and ejection rates <sup>2</sup>, strain <sup>3</sup> and morphological descriptors <sup>4</sup>. However, most of these biomarkers are not routinely used, as manually analysing all frames of a short-axis cine CMR scan is time-consuming.

In recent years, artificial intelligence (AI) methods have achieved human-level accuracy in the segmentation of short-axis cine CMR <sup>5-9</sup>. However, translation to clinical practice remains challenging for several reasons. Firstly, most AI methods lack adequate quality controls to detect errors in automatic CMR segmentations. Secondly, training datasets are often too homogenous to facilitate their widespread use. Thirdly, clinical data from different centres encompassing enough diseases and MRI vendors often suffer from intra- and inter-centre differences in data format (DICOM headers and segmentations) and label availability (presence or absence of myocardial segmentations for end-systolic images). Finally, the preferred segmentation strategy (including or excluding papillary muscles) can differ between centres applying AI methods. Most AI methods commonly ignore these challenges.

We previously developed AI-CMR<sup>QC</sup> – a comprehensive tool for processing CMR scans using quality-controlled AI – to obtain a large set of biomarkers of systolic and diastolic function with human-level accuracy and automated identification of possible erroneous results <sup>5,10</sup>. However, this tool was developed using a single-scanner, highly controlled dataset from the UK Biobank population study <sup>11</sup>. In this paper, we extend our previous work and propose a novel AI tool that can be applied to the variety of diseases, vendors and imaging protocols encountered in clinical practice, and furthermore caters for different segmentation strategies. By addressing the challenges posed by erroneous data, homogeneous training datasets, and inter-centre differences, we show that this new approach enables AI-CMR<sup>QC</sup> to robustly and automatically analyse routine clinical CMR scans.

## Methods

### Datasets

Our proposed CMR analysis tool was developed and validated using routine clinical CMR scans analysed by expert CMR cardiologists from two NHS hospitals (n=3207), known as the “NHS” dataset. The acquisition, pre-processing, and characteristics of this dataset are detailed in Supplemental Method A. Additionally, the tool was validated externally on the “Duke” clinical dataset from Duke Cardiovascular Magnetic Resonance Center, Durham, NC (n=1319); and on four public datasets of research CMR scans: UK Biobank or “UKBB” <sup>11</sup> (n=4872), “ACDC” <sup>12</sup> (n=100), “M&Ms” <sup>13</sup> (n=345), and “M&Ms-2” <sup>14</sup> (n=360). Short-axis CMR scans and manual segmentations acquired at end-diastole (ED) and end-systole (ES) were always available. Across the datasets, variation existed in segmentation strategy: in both clinical datasets, the RV and LV were not always segmented in the same frame and myocardial segmentations were not always present (particularly in ED); in the Duke dataset, papillary muscles were excluded from the LV and RV blood pools. The dataset characteristics are summarised in

Table 1. Additionally, disease and scanner information were stored for each CMR case – where available – to perform a stratified analysis.

To ensure the quality of the clinical data used for training and validation, the ground truth segmentations underwent a thorough data quality assessment (QA<sup>gt</sup>). Firstly, the NHS and Duke clinical datasets underwent the following automatic QA<sup>gt</sup> steps: duplicate segmentations – which may occur when the clinician mistakenly uploads the same ground truth segmentation multiple times – were excluded and CMR scans with less than two segmented 3D volumes (i.e., frames) were excluded. These steps were not required for the research datasets since every case contained exactly two segmented frames and there were no duplicate segmentations. Secondly, ground truth segmentations from the NHS, Duke, ACDC, M&Ms, and M&Ms-2 datasets whose ED or ES frames fulfilled at least one of several data- and knowledge-based exclusion criteria (see Supplemental Method B) underwent a manual QA<sup>gt</sup> by four expert CMR cardiologists (see Supplemental Method C).

Our study complies with the Declaration of Helsinki. Ethical approval for use of the NHS dataset was obtained from the London Dulwich Research ethics committee (ID: 19/LO/1957). The Duke data was collected as part of an ethically approved study with title 'Deidentified Cardiovascular Magnetic Resonance Images' with Duke University Research Ethics Committee reference Pro00056051 and was fully de-identified and transferred to King's College London via a data use agreement approved by both institutions. Use of the UK Biobank dataset was covered by the ethical approval from the NHS National Research Ethics Service on 17th June 2011 (Ref 11/NW/0382) and extended on 18 June 2021 (Ref 21/NW/0157) with written informed consent obtained from all participants. The other datasets are available online, under previous approval from the various host institute ethical committees.

## Automated CMR analysis tool

Our proposed CMR analysis tool consists of CMR image pre-processing steps, a deep learning (DL) method that segments the ventricles and the myocardium from short-axis cine CMR stacks, and a post-analysis quality control (QC) step (see Central Illustration). The tool outputs the segmentations for all frames of the full CMR stack together with cardiac biomarkers such as ventricular volumes, ejection fraction, and myocardial strain. We aim to make this tool available as an easy-to-use web application which will be accessed by contacting the corresponding author.

### Step 1: CMR pre-processing

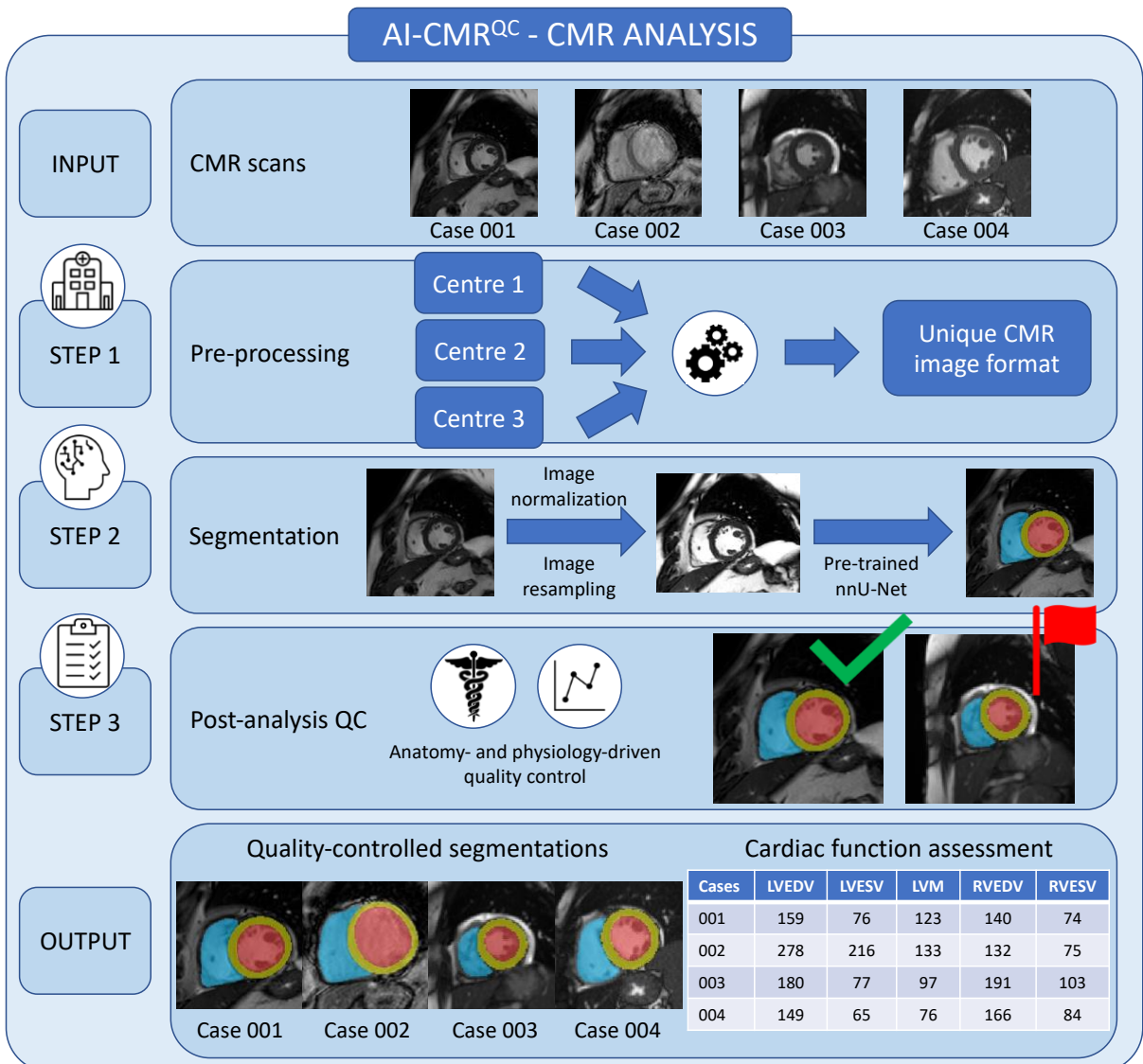
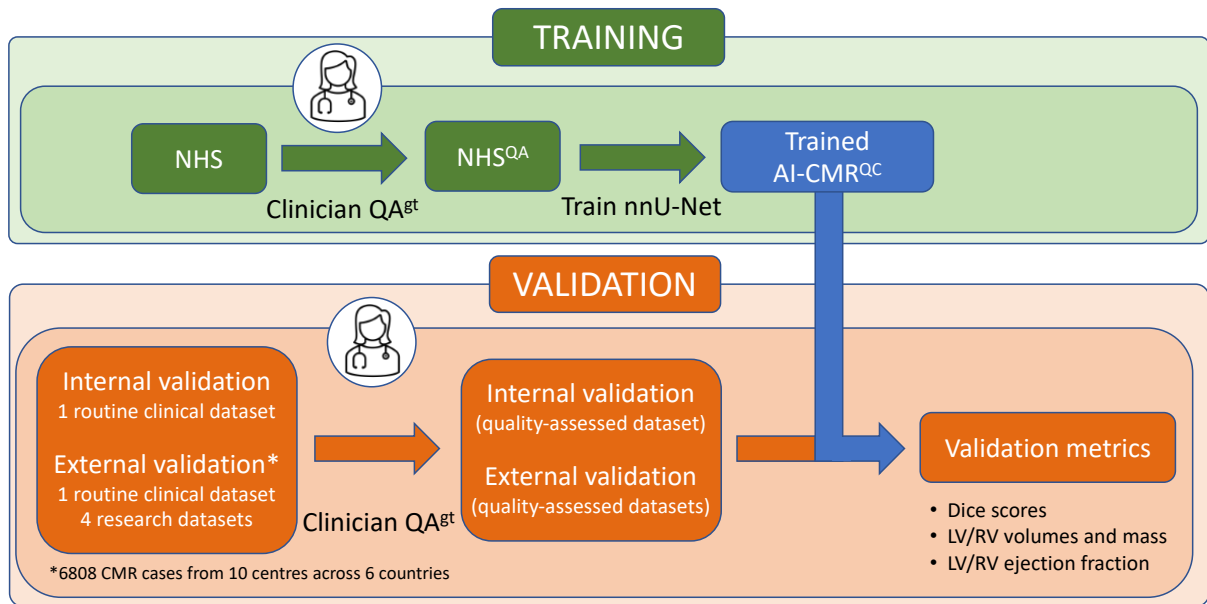
Our tool converts CMR images from all vendors and centres to a unique input format for analysis (see Supplemental Method D). This is an important but often-overlooked step, as a large variation in DICOM header information exists, which challenges the accurate translation of critical metadata such as voxel sizes and slice spacings.

**Table 1 – Internal and external dataset characteristics**

Dataset	Country	Centre	Scanner vendor	Scanner model	Disease
NHS	UK	Guy's and St Thomas' NHS Foundation Trust	Philips	Achieva 1.5T/3.0T	CHD (n=13) DCM (n=29) IHD (n=15) NOR (n=39) Other (n=50)
				Ingenia 1.5T	
			Siemens	Aera 1.5T	
Duke	US	Duke University Hospital	Siemens	Avanto 1.5T	N/A
				Sola 1.5T	
				Verio 3.0T	
				Vida 3.0T	
UKBB	UK	4 centres	Siemens	Aera 1.5T	NOR (n=4872)
ACDC	France	Centre Hospitalier Universitaire Dijon Bourgogne	Siemens	Aera 1.5T	ARV (n=30) DCM (n=30) HCM (n=30) IHD (n=30) NOR (n=30)
				Trio 3.0T	
M&Ms	Spain	Clínica Creu Blanca	Canon	Orian 1.5T	AHS (n=3) ARV (n=16) DCM (n=51) HCM (n=103) HHD (n=25) IHD (n=8) LVNC (n=4) NOR (n=125) Other (n=40)
		Hospital Universitari Dexeus	GE	Excite 1.5T	
		Clínica Sagrada Familia	Philips	Achieva 1.5T	
		Hospital Vall d'Hebron	Siemens	Avanto 1.5T	
	Germany	Universitätsklinikum Hamburg-Eppendorf	Philips	Achieva 1.5T	
Canada	McGill University Health Centre	Siemens	Skyra 3.0T		
M&Ms-2	Spain	Hospital Universitari Dexeus	GE	Excite 1.5T	ARR (n=35) DLV (n=60)* DRV (n=30) HCM (n=60)* CIA (n=35) NOR (n=75)* FALL (n=35) TRI (n=30)
				Explorer 1.5T	
				HDxt 1.5T/3.0T	
		Clínica Sagrada Familia	Philips	Achieva 1.5T	
		Hospital Vall d'Hebron	Siemens	Avanto 1.5T	
				Symphony 1.5T	
Trio 3.0T					

Dataset names, countries, centres, scanner vendors and models, and cardiac diseases.

\*These subjects were also included in M&Ms. AHS: athletic heart syndrome; ARR: congenital arrhythmogenesis; ARV: abnormal right ventricle; CIA: interatrial communication; CHD: congenital heart disease; DCM: dilated cardiomyopathy; DLV: dilated left ventricle; DRV: dilated right ventricle; FALL: tetralogy of fallot; HCM: hypertrophic cardiomyopathy; HHD: hypertensive heart disease; IHD: ischemic heart disease; LVNC: left ventricular non-compaction; NOR: normal cardiac anatomy and function; TRI: tricuspid regurgitation; UKBB: UK Biobank.



**Central Illustration** – AI-based, quality-controlled CMR analysis tool (AI-CMR<sup>QC</sup>): training, validation, and CMR analysis tool outline. QA<sup>gt</sup>: ground truth segmentation data quality assessment, QC: quality control.

## Step 2: CMR segmentation

The LV and RV endocardium and the LV myocardium are segmented from short-axis cine CMR using “nnU-Net”, a state-of-the-art medical imaging segmentation framework <sup>15</sup>. nnU-Net aims at reducing the effect of heterogeneities inherent to image data (in this study, CMR data) from different clinical centres, MRI vendors, or imaging protocols. To do so, nnU-Net automatically adapts its image pre-processing (z-score intensity normalisation and image resampling), network architecture, and hyperparameters to any given image dataset. These strategies allow nnU-Net to outperform most DL methods (even highly specialised ones) in international medical image segmentation challenges. Additionally, we modified nnU-Net’s loss function to also tackle the problem of inconsistent image labelling (e.g., missing LV myocardium segmentations). More details on nnU-Net and our loss function improvement are shown in Supplemental Method E.

An optional step allows the exclusion of papillary muscles from the LV and RV blood pool segmentations using Otsu’s threshold method <sup>16</sup>. This step was used for the Duke dataset, to cater for the segmentation strategy followed when forming Duke’s ground truth data (see Supplemental Figure 1).

## Step 3: Post-analysis QC

In our previous work, we used physiological priors for post-analysis QC. We have extended this into a larger set of QCs, based on general knowledge of the anatomy and physiology of the heart. This post-analysis QC detects segmentations that (i) are discontinuous (e.g., non-segmented slices between segmented slices), (ii) do not adhere to the anatomical relationship between the ventricles and the myocardium, (iii) are disconnected from the rest of the heart. Additionally, this QC is combined with our previously developed QC to detect physiologically implausible cardiac biomarker values or volume curve shapes. Segmentations failing this QC are flagged up for clinician review (see Supplemental Method F).

## Training

We trained nnU-Net on a subset of randomly selected cases from the NHS dataset (n=2793) using five-fold cross-validation. Consequently, nnU-Net was used as an ensemble of the five models resulting from this cross-validation.

## Validation and statistical analysis

We performed an internal validation of our tool using the remaining NHS cases that were not used for training (n=414). Subsequently, we performed an external validation in five additional datasets (n=6808) which included clinical CMR scans of patients with a range of diseases acquired at 10 international centres using 1.5 and 3T CMR scanners from all major vendors (Canon Medical Systems Corporation, Otawara, Tochigi, Japan; General Electric Healthcare, Chicago, Illinois, USA; Philips Healthcare, Best, the Netherlands; Siemens Healthineers, Erlangen, Germany).

As part of the validation, Dice scores were used to assess the agreement between the automated and manual segmentations. A Dice score of 0% indicates no agreement and a Dice score of 100% indicates perfect agreement. To provide validation metrics in a clinically meaningful way, we calculated absolute errors (i.e.,  $|automated - ground\ truth|$ ) in end-



diastolic volume (EDV), end-systolic volume (ESV), ejection fraction (EF), and left ventricular mass (LVM). Individual Dice and error distributions were tested for symmetry via visual inspection using box plots and are reported using median (interquartile range) values.

Mann-Whitney U tests were performed to compare both the Dice scores and the cardiac biomarker errors between the NHS validation cases and the external validation datasets. Additionally, we used Bland-Altman analysis and Pearson's Correlation Coefficients to evaluate the performance of our method versus manual analysis for all CMR cases. Finally, we used box plots to compare performance over major groups of cardiac diseases and scanner vendors for CMR cases. Wilcoxon sign-ranked tests were applied to determine whether there were significant errors in biomarker estimations for the different disease and CMR vendor groups. *Post hoc* testing was performed using Bonferroni correction for multiple comparisons.

## Results

As a result of the quality control of ground truth images, between 2% and 19% of CMR cases were discarded for each dataset. A detailed description of the reasons why these CMR cases were discarded is provided in Supplemental Method C.

### Dice

For the internal NHS dataset, median Dice scores between the automated and manual segmentation were 94.3% for the LV blood pool (LVBP), 85.5% for the LV myocardium (MYO), and 90.8% for the RV blood pool (RVBP) segmentations. For the external datasets, median Dice scores of the automated compared to manual segmentation were >91.3% for the LVBP, >83.0% for the MYO, and >87.4% for the RVBP segmentations. Dice scores for each dataset and cardiac label are shown in Table 2. Additionally, Dice scores for each scanner model and cardiac label are shown in Supplemental Table 1.

### Cardiac biomarkers

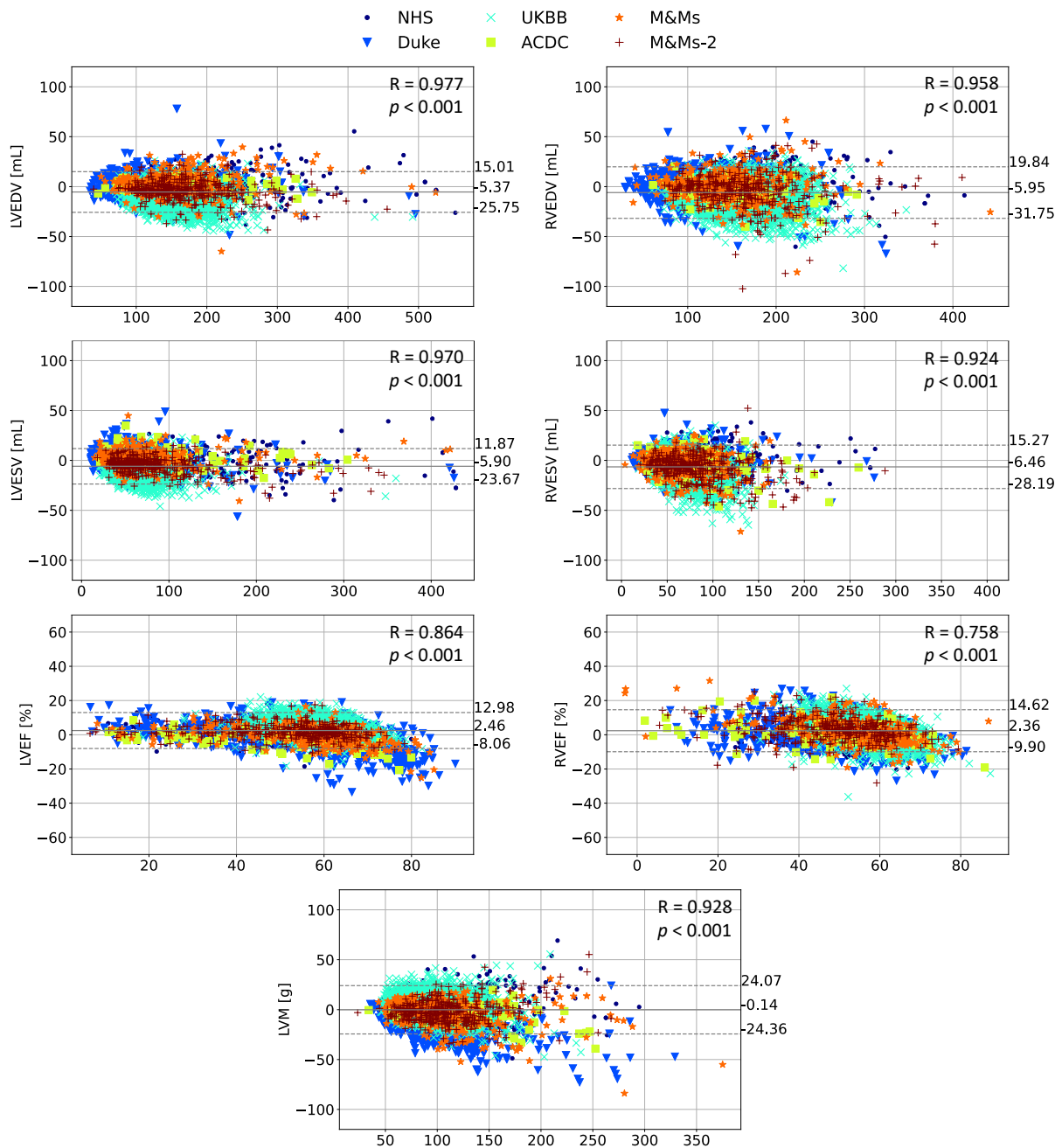
A Bland-Altman analysis of the differences between cardiac biomarkers derived from the automated and manual segmentations is shown in Figure 1. For the internal NHS dataset, median absolute errors in cardiac biomarkers were 6.7mL for LVEDV, 6.3mL for LVESV, 3.4% for LVEF, 8.9g for LVM, 8.5mL for RVEDV, 6.4mL for RVESV, and 4.2% for RVEF. For the external datasets, median absolute errors in cardiac biomarkers were <7.3mL for LVEDV, <8.4mL for LVESV, <5.3% for LVEF, <13.3g for LVM, <9.2mL for RVEDV, <8.9mL for RVESV and <5.9% for RVEFI.

Table 3 shows, for each dataset, the ground truth values (first row) and the median (interquartile range) absolute errors (second row) of the automated analysis. There are statistically significant differences in performance between the internal NHS validation cases and the external validation datasets. The box plots in Figure 2 and 3 show the errors between ground truth and automated cardiac biomarkers grouped by cardiac disease and scanner type, with the largest errors found in healthy (NOR) subjects and Siemens scanners, respectively. Similar box plots grouped by magnetic field strength are shown in Supplemental Figure 2.

**Table 2 – Dice scores of automated vs manual segmentations**

<b>Dataset</b>	<b>LVBP [%]</b>	<b>MYO [%]</b>	<b>RVBP [%]</b>	<b>Average [%]</b>
NHS	94.3 (4.0)	85.5 (4.4)	90.8 (5.4)	91.3 (7.5)
Duke	91.3 (6.5) <sup>***</sup>	83.0 (4.8) <sup>***</sup>	89.3 (6.8) <sup>***</sup>	89.2 (8.3) <sup>***</sup>
UKBB	91.8 (5.9) <sup>***</sup>	83.0 (6.5) <sup>***</sup>	87.8 (7.8) <sup>***</sup>	87.4 (8.9) <sup>***</sup>
ACDC	95.5 (3.9)	87.4 (3.5) <sup>***</sup>	91.8 (7.0) <sup>*</sup>	90.6 (7.9)
M&Ms	93.4 (5.4) <sup>***</sup>	85.4 (5.7)	90.4 (6.8)	89.4 (8.3) <sup>***</sup>
M&Ms-2	94.6 (4.2)	86.0 (5.6) <sup>*</sup>	90.9 (6.7)	90.3 (8.3) <sup>**</sup>

Dice scores are shown as median (interquartile range) percentages for each validation dataset, including values per label and their average. Comparisons between the Dice scores of the NHS validation cases and the external validation datasets were performed using Mann-Whitney U tests. Pairwise *post hoc* testing was performed using Bonferroni correction for multiple comparisons. Asterisks indicate statistically significant differences for each label after correction (20 tests), where \* =  $p < 0.01/20$ , \*\* =  $p < 0.001/20$ , \*\*\* =  $p < 0.0001/20$ . LVBP: LV blood pool, MYO: LV myocardium, RVBP: RV blood pool.



**Figure 1 – Bland-Altman analysis of cardiac volume, ejection fraction, and mass:** Cardiac biomarkers derived from manual and automated segmentations were compared for all validation cases. The thick line depicts the mean bias between the automated and manual analysis. The top and bottom dotted lines correspond to +1.96 and -1.96 standard deviations from the mean bias, respectively. The Pearson's Correlation Coefficients (R) between our method and the manual analysis (and the corresponding  $p$ -values) are indicated for each cardiac biomarker. LVEDV: left ventricular end-diastolic volume; LVESV: left ventricular end-systolic volume; LVEF: left ventricular ejection fraction; LVM: left ventricular mass; RVEDV: right ventricular end-diastolic volume; RVEF: right ventricular ejection fraction; and RVESV: right ventricular end-systolic volume.

**Table 3 – Errors between cardiac biomarkers derived from automated and manual segmentations**

Dataset	LV				RV		
	EDV [mL]	ESV [mL]	EF [%]	LVM [g]	EDV [mL]	ESV [mL]	EF [%]
NHS	198.8 (75.3)	108.9 (70.3)	48.7 (14.0)	116.5 (42.6)	172.4 (52.4)	84.6 (40.3)	52.3 (9.8)
	6.7 (13.5)	6.3 (12.9)	3.4 (4.3)	8.9 (17.9)	8.5 (15.8)	6.4 (12.5)	4.2 (5.4)
Duke†	107.7 (46.6)	50.7 (38.2)	55.9 (14.8)	107.4 (46.1)	104.6 (41.4)	52.6 (28.3)	51.0 (11.2)
	5.7 (11.0)***	5.0 (9.7)	5.3 (7.1)***	13.3 (17.2)***	6.0 (11.8)***	4.5 (9.1)***	5.2 (6.8)**
UKBB	149.0 (34.9)	62.0 (20.7)	58.8 (6.3)	91.9 (25.4)	155.6 (37.5)	69.1 (22.7)	56.1 (6.4)
	7.3 (12.5)***	8.4 (9.6)***	4.7 (4.2)***	6.6 (12.8)**	9.2 (14.7)***	8.9 (12.5)***	5.3 (5.9)***
ACDC	161.4 (67.6)	94.0 (71.0)	47.6 (18.8)	126.7 (50.1)	151.7 (51.2)	86.1 (51.1)	46.1 (18.1)
	3.6 (5.8)	5.3 (8.0)***	4.6 (5.1)***	6.8 (12.7)***	6.1 (11.2)***	5.7 (11.1)**	5.6 (7.6)
M&Ms	159.1 (61.1)	73.0 (54.2)	56.9 (13.7)	115.9 (49.1)	147.4 (49.9)	69.5 (37.4)	53.9 (12.2)
	6.2 (13.4)	5.1 (9.8)***	4.2 (5.4)***	8.2 (16.6)***	8.4 (16.9)	5.9 (13.7)***	5.6 (7.3)***
M&Ms-2	174.9 (61.6)	89.6 (58.9)	52.0 (13.7)	112.0 (36.7)	169.1 (56.5)	89.5 (42.1)	48.3 (12.8)
	6.3 (9.6)***	5.5 (8.4)***	3.4 (4.2)	7.3 (14.2)***	8.7 (16.5)***	8.3 (13.9)***	5.9 (7.0)***

For each validation dataset, the first row (highlighted in grey) reports the ground truth clinical measurements for each cardiac biomarker as median (interquartile range). The second row reports the median absolute errors (interquartile range) between cardiac biomarkers derived from the automated and ground truth segmentations. Comparisons between the errors of the NHS validation cases and the external validation datasets were performed using Mann-Whitney U tests. Pairwise *post hoc* testing was performed using Bonferroni correction for multiple comparisons. Asterisks indicate statistically significant differences for each biomarker after correction (35 tests), where \* =  $p < 0.01/35$ , \*\* =  $p < 0.001/35$ , \*\*\* =  $p < 0.0001/35$ . † Lower ventricular volumes in the Duke dataset are due to the exclusion of papillary muscle from the ground truth segmentations. LV: left ventricle, RV: right ventricle, EDV: end-diastolic volume, ESV: end-systolic volume, EF: ejection fraction, LVM: left ventricular mass.

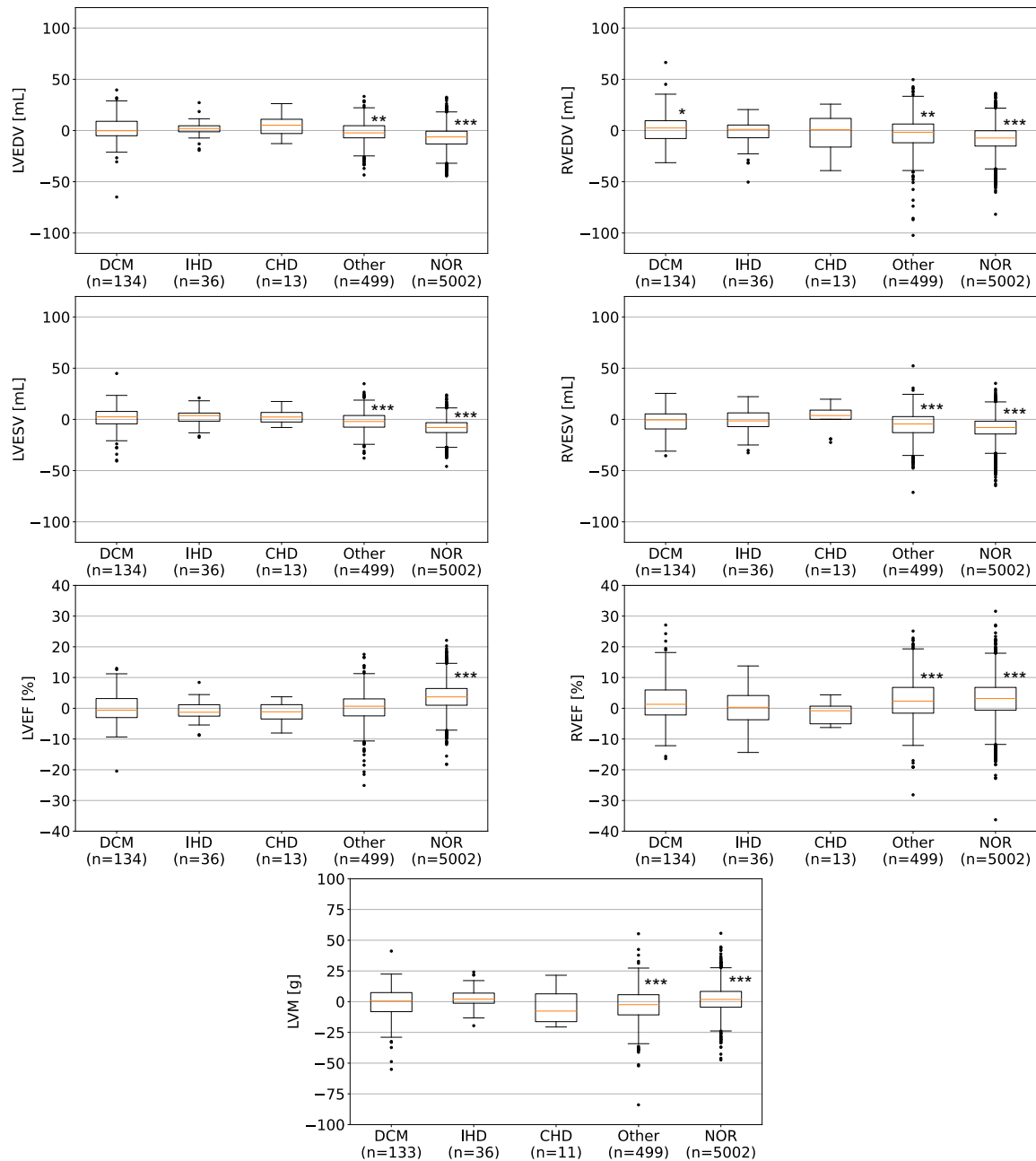


**Figure 2 – Box plots of manually and automatically derived cardiac biomarkers for each disease group:** Statistical differences from zero were assessed using Wilcoxon sign-ranked tests. Pairwise *post hoc* testing was performed using Bonferroni correction for multiple comparisons. Asterisks indicate statistically significant differences from zero for each group after correction (five tests), where \* =  $p < 0.01/5$ , \*\* =  $p < 0.001/5$ , \*\*\* =  $p < 0.0001/5$ . CHD: Congenital Heart Disease; DCM: Dilated Cardiomyopathy; IHD: Ischemic Heart Disease; LVEDV: left ventricular end-diastolic volume; LVESV: left ventricular end-systolic volume; LVEF: left ventricular ejection fraction; LVM: left ventricular mass; NOR: Normal Cardiac Anatomy and Function; Other: other cardiac diseases; RVEDV: right ventricular end-diastolic volume; RVEF: right ventricular ejection fraction; and RVESV: right ventricular end-systolic volume.

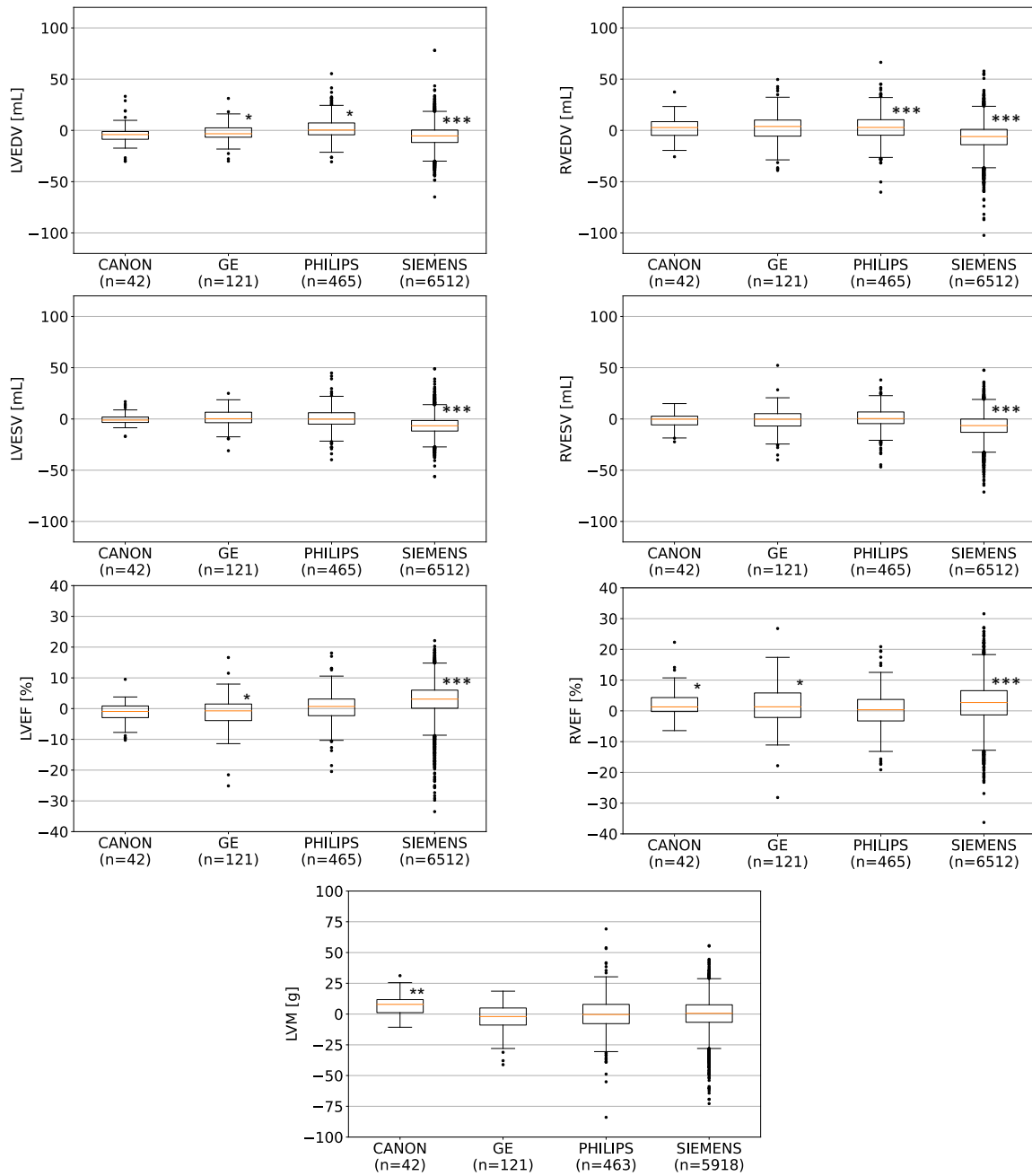


**Figure 3 – Box plots of manually and automatically derived cardiac biomarkers for each scanner group:** Statistical differences from zero were assessed using Wilcoxon sign-ranked tests. Pairwise *post hoc* testing was performed using Bonferroni correction for multiple comparisons. Asterisks indicate statistically significant differences from zero for each group after correction (four tests), where \* =  $p < 0.01/4$ , \*\* =  $p < 0.001/4$ , \*\*\* =  $p < 0.0001/4$ . Abbreviations as in Figure 2.

## Discussion

In this paper, we have extended our previous quality-controlled AI pipeline for automated CMR analysis (AI-CMR<sup>QC</sup>)<sup>5,10</sup>. We have improved the deep learning segmentation framework to tackle clinical data heterogeneity and developed several quality control steps to detect potentially erroneous segmentations. The tool was developed and validated using 7222 CMR cases containing a wide range of cardiac diseases, scanner models, field strengths, centres, and clinical experience. Compared to previous works, we have validated our tool on two large clinical datasets containing routine CMR exams (n=1270 and n=414) and on four external research datasets (n=4787, n=345, n=324, and n=82).

We have performed an extensive external validation which has shown that AI-CMR<sup>QC</sup> now achieves human-level accuracy for short-axis cine CMR segmentation across a wide range of diseases, vendors, and clinical imaging protocols. Our method yielded median Dice scores of >91%, >83%, and >87% for the LVBP, LVM, and RVBP, respectively, translating into median absolute errors in cardiac biomarkers of <8.4mL for the LV, <9.2mL for the RV <13.3g for the LVM, and <5.9% for EF across all datasets.

We examined the performance of our method over different phenotypes of cardiac disease (see Figure 2). Performance was good across different disease groups, including the spectrum of cardiomyopathic diseases, in addition to several congenital cases such as pulmonary arterial hypertension and tetralogy of Fallot (see Figure 4 for examples). Although the errors were significantly different from zero in some groups, they were within the ranges of inter-observer variability in manual CMR analysis<sup>17,18</sup>, and are therefore similar to those experienced in clinical practice; the worst-performing phenotype (healthy subjects – NOR category in Figure 2) had median absolute errors of <10mL for volumes and <5% for EF. Most healthy subjects came from the UK Biobank dataset, whose segmentations were obtained using a stringent standardized operating procedure whereby each analyst was purposely trained to limit inter-observer variability, thus leading to a systematic segmentation style. This could explain why this group had the highest bias in our analysis. The training dataset (NHS) is likely to reflect inter-observer variability among different CMR cardiologists, which also exists in all validation datasets except for the UK Biobank. A complete analysis of congenital disease phenotypes is beyond the scope of the current work but will be the subject of a future study. These results show that our tool performs well for a typical (non-congenital) cardiac MR list.

Our method also performed well across all scanner types (see Figure 3), including those not seen during training (Canon and GE). The largest error was found in Siemens data, but this error was again within observed inter-observer variability in CMR analysis<sup>17,18</sup>. Again, this is likely explained by the systematic difference in segmentation style between the UK Biobank data – which was acquired using a single Siemens scanner model – and the NHS data. The performance of our method is comparable to previously published AI algorithms trained and validated using only a single dataset<sup>5,9</sup>. One recent study used multi-centre, multi-vendor data for training<sup>7</sup>; however, it did not include Canon scanners and lacked quality controls, which potentially leads to better results (see next section in the discussion). Furthermore, it only validated externally using a single-centre, single-scanner dataset.

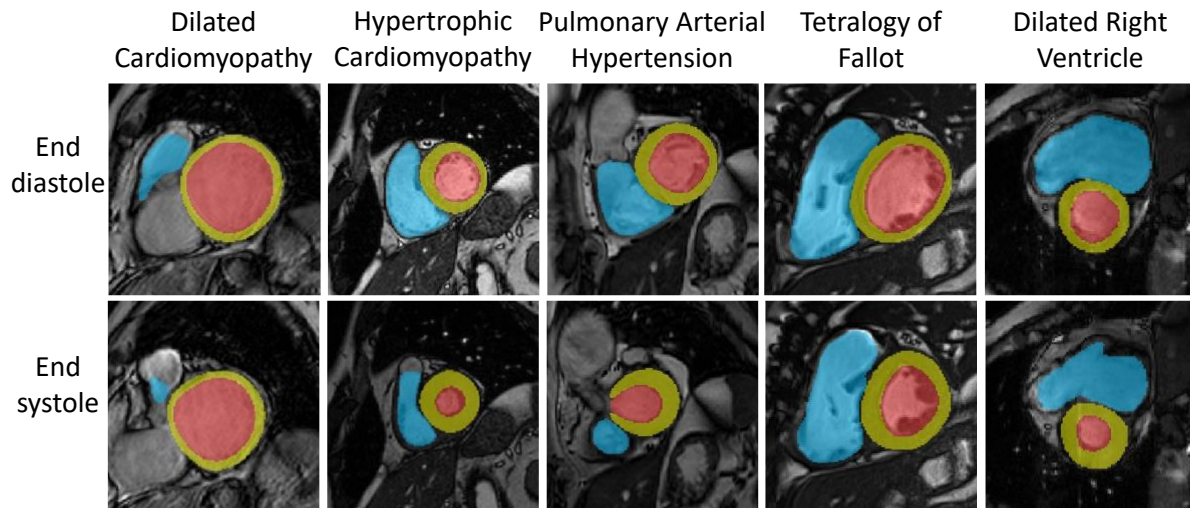


**Figure 4 – Examples of automated segmentations from different disease groups:** The middle slice of each automated segmentation is shown in ED and ES. Cardiac labels: LV blood pool (red), LV myocardium (yellow) and RV blood pool (blue).

## Generalisable DL models and diverse CMR data

Although recent works on automated CMR analysis have shown excellent results in highly controlled (e.g., same clinician, scanner model, or CMR protocol) public datasets, these methods tend to generalise poorly to other domains<sup>19</sup>. DL models are highly sensitive to data – even minor image differences can impact performance significantly. Even if generalisable DL models are deployed, their validation should still be performed using diverse, routine clinical data to avoid any risk of bias. Unfortunately, no sufficiently large multi-centre, multi-disease training datasets are currently available, partly due to ethical restrictions and challenges in extracting and processing such large datasets from clinical storage. To address such limitations, this study has aggregated CMR data from two UK hospitals, one US hospital, and several external research datasets. We engineered a pipeline which can handle data from different sources, and which includes automated detection and selection of short-axis cine images from CMR scans<sup>10</sup> and conversion of images and segmentations to a standard format. This combined dataset allowed robust validation of our tool.

In this paper, we adapted and implemented nnU-Net, a state-of-the-art DL framework that integrates a set of image pre-processing techniques that improve its generalisability. We showed that the performance of our tool remained good in a large and heterogeneous external validation dataset. This shows the ability of the nnU-Net framework to generalise well to unseen data when trained using a sufficiently heterogeneous training set. Reducing the generalisation ‘brittleness’ of AI models (a term coined for unexpected performance drops due to slight data differences that seem unimportant to human observers) is of crucial importance for safe implementation in clinical practice<sup>20</sup>.

## Quality-controlled AI

Most commercial cardiac analysis software has already implemented AI algorithms. However, most of these algorithms are still not optimised for generalisation and suffer from reduced performance when applied to other datasets<sup>19,21</sup>. Therefore, these tools require continuous clinician oversight, which is sufficient and desirable for prospective clinical reporting. However,



in the current era of big data, AI tools that can analyse large (retrospective) datasets or registries robustly are essential for developing clinical research. Our AI-CMR<sup>QC</sup> tool includes robust post-analysis QC steps – independent of the DL-based segmentation algorithm – that flag up potential analysis errors with high sensitivity<sup>5</sup>. Our current validation study shows that AI-CMR<sup>QC</sup> performs well overall for all major vendors, scanning protocols and cardiac disease groups. Thus, this is a suitable option for analysing large CMR research datasets. To prevent a potential bias in the validation, we did not exclude any of the cases that were flagged up by the post-analysis QC of AI-CMR<sup>QC</sup>. In prospective use, flagged up cases would be reviewed by clinicians and accepted or rejected (and redrawn), so real-life results could only be better compared to the current validation results.

## The importance of ground truth data quality

The quality of the ground truth segmentations is of utmost importance when developing and evaluating DL methods. Therefore, we performed stringent automated and manual data quality assessments (QA<sup>gt</sup>) on all datasets, except for the highly controlled UK Biobank dataset. Firstly, we automatically identified ground truth segmentations presenting non-physiological discontinuities, missing or erroneous labels, and large stroke volume differences. Secondly, these cases were manually assessed by expert CMR clinicians and discarded where appropriate. See Supplemental Methods B and C for a more detailed description of the QA<sup>gt</sup> steps applied to the ground truth segmentations, respectively.

The importance of applying this QA<sup>gt</sup> to the training and validation data is twofold. Firstly, we excluded erroneous ground truth segmentations (e.g., a partial segmentation that was stored halfway through the manual analysis and was never completed by the clinician) from the clinical datasets. Secondly, we found that the online external validation datasets (i.e., ACDC, M&Ms and M&Ms-2) also exhibited ground truth quality issues in a non-negligible number of cases. Segmentation quality did not always adhere to the clinical standards for ventricular segmentation for volume quantification published by the European and American CMR societies<sup>22,23</sup>. Commonly, issues were found at the base of the RV, which sometimes was not segmented (see Figure 5). Moreover, in some cases the short-axis cine sequences did not cover the full heart (the basal slices were absent). Since the basal slices are challenging for segmentation algorithms, missing basal slices have direct implications on validation results.

Our QA<sup>gt</sup> of the ground truth segmentations from the external validation datasets led to the exclusion of 4-18% of cases, depending on the dataset (see Supplemental Table 2). The ACDC, M&Ms and M&Ms-2 datasets have become standard datasets for external validation of clinical CMR segmentation algorithms. However, these datasets were initially developed within the engineering community and were never intended to provide the robustness and high-quality standards for real-world clinical validation. The results of our QA<sup>gt</sup> have highlighted the importance of scrutinising such external datasets and we therefore call for the development of high-quality benchmark datasets by the clinical community. For completeness and retrospective evaluation against previously published results, we have included the performance of our method on the full original external datasets in Supplemental Tables 3 and 4.

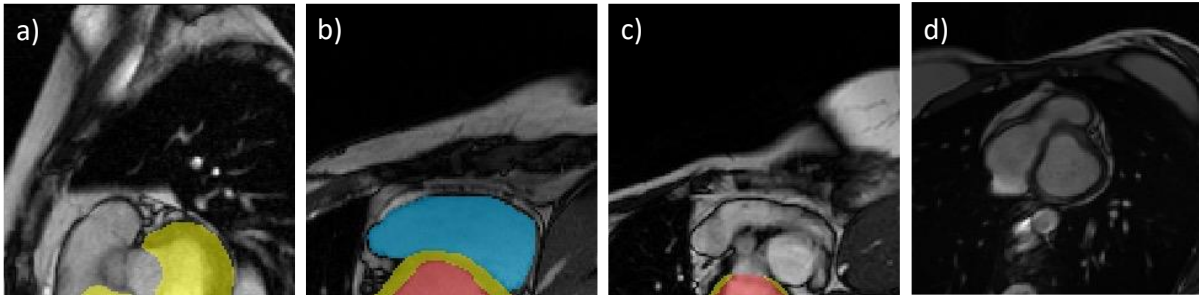


**Figure 5 – Examples of erroneous ground truth segmentations identified during manual QA<sup>gt</sup>:** Cardiac labels: LV blood pool (red), LV myocardium (yellow) and RV blood pool (blue). a) Image in ED: note that the LV myocardium is segmented, but the LV blood pool segmentation is absent and that the RV segmentation is labelled as myocardium (yellow); b) top slice of the cine stack in ED: the basal part of the heart is not included in the cine SAX stack; c) image in ED: note the unusual LV structure that was segmented and the absence of an RV segmentation; d) image in ES; note the absence of LV and RV segmentations, while myocardium is present for both.

## Inconsistent image labels in clinical CMR

Working with routine clinical CMR scans has highlighted the importance of accounting for inconsistent image labelling. For example, the LV myocardium is often only segmented in diastole, not in systole, and the RV and LV blood pools can sometimes be segmented in different frames. This makes training accurate DL segmentation methods on clinical scans challenging, as it misleads them into learning missing labels as background. Although several works have addressed these inconsistencies<sup>24,25</sup>, this issue is commonly ignored. We have tackled this challenge by modifying the nnU-Net’s loss function (see Supplementary Method E). With this modification, we achieved similar segmentation performance for labels that are always present (e.g., LV and RV blood pools) and for those that appear much less often (e.g., LV myocardium in ES).

## Dealing with papillary muscles

Different protocols are used when segmenting short-axis cine CMR images. Some CMR departments include papillary muscles in the LV and RV blood pools, while others exclude them. This depends both on clinician preference and on the segmentation technique used (e.g., drawing myocardial borders manually or semi-automatically using region growing)<sup>23</sup>. Our tool was originally trained to include papillary muscles in the ventricular blood pools. However, papillary muscles were excluded from the segmentation in the Duke external validation dataset. Therefore, we developed and applied an automatic image thresholding technique – based on Otsu’s method – to the segmented blood pools to obtain segmentations that exclude the papillary muscles. This did not only allow external validation in the Duke dataset but also allows users of our tool to choose their preferred segmentation strategy.

## Limitations

Although we trained our segmentation algorithm on a large clinical dataset (n=2793), this dataset did not contain all possible diseases, CMR vendors, or imaging protocols. In particular, it did not include complex congenital heart diseases, although it did incorporate a significant

number of inherited diseases that encompass variation in ventricular shape and function. Similarly, our five external validation datasets are not all-encompassing. In the future, we aim to deploy our method in other centres to perform additional validation steps throughout this deployment to ensure the tool's robustness and to improve its performance. Finally, the current version of the tool can only be used to analyse short-axis CMR scans. Future work could extend the tool to be used with long-axis cine CMR.

Potential weaknesses in DL models remain hard to anticipate, due to their black-box configuration. Model interpretability and visualisation techniques could potentially further help to address this limitation.

## Conclusions

We have developed AI-CMR<sup>QC</sup>, an AI-based tool for quality-controlled, automated analysis of short-axis CMR scans. We implemented a state-of-the-art DL method that significantly reduces performance drop for CMR images not seen during training. We validated our tool using over 7000 CMR cases from multiple centres and countries and showed that our method yields human-level accuracy for LV and RV segmentations for all major CMR scanner vendors, and for a wide range of cardiac disease phenotypes and acquisition protocols.

## Perspectives

**CLINICAL COMPETENCIES:** Deep learning (DL) models suffer from generalisation challenges. We show that combining new data processing techniques and robust QC of training data yields human-level accuracy of DL-based segmentation in all major disease groups, scanner vendors, and CMR protocols.

**TRANSLATIONAL OUTLOOK:** AI-CMR<sup>QC</sup> allows quality-controlled analysis of CMR images to obtain biomarkers of cardiac function. This tool can be used by the research community to process large datasets of CMR scans and provides comprehensive cardiac biomarkers for clinical research.

## References

1. von Knobelsdorff-Brenkenhoff F, Pilz G, Schulz-Menger J. Representation of cardiovascular magnetic resonance in the AHA / ACC guidelines. *Journal of Cardiovascular Magnetic Resonance*. 2017;19(1):70. doi:10.1186/s12968-017-0385-z
2. Maceira A, Prasad S, Khan M, Pennell D. Normalized Left Ventricular Systolic and Diastolic Function by Steady State Free Precession Cardiovascular Magnetic Resonance. *Journal of Cardiovascular Magnetic Resonance*. 2006;8(3):417-426. doi:10.1080/10976640600572889
3. Claus P, Omar AMS, Pedrizzetti G, Sengupta PP, Nagel E. Tissue Tracking Technology for Assessing Cardiac Mechanics. *JACC: Cardiovascular Imaging*. 2015;8(12):1444-1460. doi:10.1016/j.jcmg.2015.11.001
4. Medrano-Gracia P, Cowan BR, Ambale-Venkatesh B, et al. Left ventricular shape variation in asymptomatic populations: the multi-ethnic study of atherosclerosis. *Journal of Cardiovascular Magnetic Resonance*. 2014;16(1):56. doi:10.1186/s12968-014-0056-2
5. Ruijsink B, Puyol-Antón E, Oksuz I, et al. Fully Automated, Quality-Controlled Cardiac Analysis From CMR. *JACC: Cardiovascular Imaging*. 2020;13(3):684-695. doi:10.1016/j.jcmg.2019.05.030
6. Puyol-Antón E, Ruijsink B, Baumgartner CF, et al. Automated quantification of myocardial tissue characteristics from native T1 mapping using neural networks with uncertainty-based quality-control. *Journal of Cardiovascular Magnetic Resonance*. 2020;22(1):60. doi:10.1186/s12968-020-00650-y
7. Davies RH, Augusto JB, Bhuva A, et al. Precision measurement of cardiac structure and function in cardiovascular magnetic resonance using machine learning. *Journal of Cardiovascular Magnetic Resonance*. 2022;24(1):16. doi:10.1186/s12968-022-00846-4
8. Fadil H, Totman JJ, Hausenloy DJ, et al. A deep learning pipeline for automatic analysis of multi-scan cardiovascular magnetic resonance. *Journal of Cardiovascular Magnetic Resonance*. 2021;23(1):47. doi:10.1186/s12968-020-00695-z
9. Bai W, Sinclair M, Tarroni G, et al. Automated cardiovascular magnetic resonance image analysis with fully convolutional networks. *Journal of Cardiovascular Magnetic Resonance*. 2018;20(1):65. doi:10.1186/s12968-018-0471-x
10. Vergani V, Razavi R, Puyol-Antón E, Ruijsink B. Deep Learning for Classification and Selection of Cine CMR Images to Achieve Fully Automated Quality-Controlled CMR Analysis From Scanner to Report. *Frontiers in Cardiovascular Medicine*. 2021;8. doi:10.3389/fcvm.2021.742640
11. Petersen SE, Matthews PM, Francis JM, et al. UK Biobank's cardiovascular magnetic resonance protocol. *Journal of Cardiovascular Magnetic Resonance*. 2015;18(1):8. doi:10.1186/s12968-016-0227-4
12. Bernard O, Lalande A, Zotti C, et al. Deep Learning Techniques for Automatic MRI Cardiac Multi-Structures Segmentation and Diagnosis: Is the Problem Solved? *IEEE Transactions on Medical Imaging*. 2018;37(11):2514-2525. doi:10.1109/TMI.2018.2837502
13. Campello VM, Gkontra P, Izquierdo C, et al. Multi-Centre, Multi-Vendor and Multi-Disease Cardiac Segmentation: The M&Ms Challenge. *IEEE Transactions on Medical Imaging*. 2021;40(12):3543-3554. doi:10.1109/TMI.2021.3090082

14. Martín-Isla C, Lekadir K. Multi-Disease, Multi-View & Multi-Center Right Ventricular Segmentation in Cardiac MRI (M&Ms-2). Accessed May 20, 2022. <https://www.ub.edu/mnms-2/>
15. Isensee F, Jaeger PF, Kohl SAA, Petersen J, Maier-Hein KH. nnU-Net: a self-configuring method for deep learning-based biomedical image segmentation. *Nature Methods*. 2021;18(2):203-211. doi:10.1038/s41592-020-01008-z
16. Otsu N. A Threshold Selection Method from Gray-Level Histograms. *IEEE Transactions on Systems, Man, and Cybernetics*. 1979;9(1):62-66. doi:10.1109/TSMC.1979.4310076
17. Childs H, Ma L, Ma M, et al. Comparison of long and short axis quantification of left ventricular volume parameters by cardiovascular magnetic resonance, with ex-vivo validation. *Journal of Cardiovascular Magnetic Resonance*. 2011;13(1):40. doi:10.1186/1532-429X-13-40
18. Luijnenburg SE, Robbers-Visser D, Moelker A, Vliegen HW, Mulder BJ, Helbing WA. Intra-observer and interobserver variability of biventricular function, volumes and mass in patients with congenital heart disease measured by CMR imaging. *Journal of Cardiovascular Magnetic Resonance*. 2009;11(S1):P100. doi:10.1186/1532-429X-11-S1-P100
19. Leiner T, Rueckert D, Suinesiaputra A, et al. Machine learning in cardiovascular magnetic resonance: basic concepts and applications. *Journal of Cardiovascular Magnetic Resonance*. 2019;21(1):61. doi:10.1186/s12968-019-0575-y
20. Kelly CJ, Karthikesalingam A, Suleyman M, Corrado G, King D. Key challenges for delivering clinical impact with artificial intelligence. *BMC Medicine*. 2019;17(1):195. doi:10.1186/s12916-019-1426-2
21. Wang S, Patel H, Miller T, et al. AI Based CMR Assessment of Biventricular Function. *JACC: Cardiovascular Imaging*. 2022;15(3):413-427. doi:10.1016/j.jcmg.2021.08.011
22. Petersen SE, Khanji MY, Plein S, Lancellotti P, Bucciarelli-Ducci C. European Association of Cardiovascular Imaging expert consensus paper: a comprehensive review of cardiovascular magnetic resonance normal values of cardiac chamber size and aortic root in adults and recommendations for grading severity. *European Heart Journal - Cardiovascular Imaging*. 2019;20(12):1321-1331. doi:10.1093/ehjci/jez232
23. Schulz-Menger J, Bluemke DA, Bremerich J, et al. Standardized image interpretation and post-processing in cardiovascular magnetic resonance - 2020 update. *Journal of Cardiovascular Magnetic Resonance*. 2020;22(1):19. doi:10.1186/s12968-020-00610-6
24. Petit O, Thome N, Charnoz A, Hostettler A, Soler L. Handling Missing Annotations for Semantic Segmentation with Deep ConvNets. In: ; 2018:20-28. doi:10.1007/978-3-030-00889-5\_3
25. Fidon L, Aertsen M, Emam D, et al. Label-Set Loss Functions for Partial Supervision: Application to Fetal Brain 3D MRI Parcellation. In: ; 2021:647-657. doi:10.1007/978-3-030-87196-3\_60

# Supplemental Appendix

## Supplemental Methods

### A. NHS dataset acquisition, pre-processing, and quality assessment

For the NHS dataset, clinical CMR scans and corresponding segmentations were automatically downloaded from the Guy's and St Thomas' NHS Foundation Trust PACS, sorted according to their acquisition sequence, and anonymised. They were then converted from a DICOM format to a NIFTI format as required by the tool, duplicate or empty ground truth segmentations were removed, end-diastolic and end-systolic frames were identified, and a thorough data quality assessment (QA<sup>gt</sup>) was applied to the ground truth segmentations from both frames. A summary of this process, including the number of cases discarded in each step, is provided in Supplemental Figure 3. The manual segmentations (i.e., left ventricular endocardium and myocardium and right ventricular endocardium) were acquired using the commercially available cvi42 CMR analysis software (Circle Cardiovascular Imaging Inc., Calgary, Alberta, Canada, version 5.10.1).

### B. Automated quality assessment of ground truth segmentations

The ground truth statistics from the UKBB, ACDC, M&Ms, and M&Ms-2 datasets (shown in Supplemental Table 5) together with clinical knowledge were used to establish the following criteria to identify potentially erroneous ground truth segmentations:

- containing unexpected labels - other than LVBP, MYO, or RVBP;
- one of its ventricular volumes being equal to zero;
- disagreement between image and segmentation metadata (e.g., different voxel size or orientation);
- containing outliers (i.e., voxels disconnected from the main segmentation) representing more than 10% of the total number of segmented voxels - this step was first applied to a combination of all segmented labels and then to each individual label;
- any label appearing in less than 30% of segmented slices;
- presence of non-segmented slices between segmented slices for any label;
- negative or zero LV or RV stroke volume; or
- LV and RV stroke volume differences larger than 25%.

Finally, outliers representing less than 10% of the segmented voxels were automatically removed, keeping only the largest connected component for each label.

### C. Manual quality assessment of ground truth segmentations

The potentially erroneous ground truth segmentations from the NHS, Duke, ACDC, M&Ms, and M&Ms-2 datasets underwent a manual QA<sup>gt</sup> that uncovered major issues in some cases. The number of excluded cases per dataset and the corresponding exclusion criteria are detailed below:

- NHS: 832 cases were excluded due to severe CMR artefacts affecting the cardiac region in any slice; ICD, pacemaker lead or sternal wires; segmentations including the atria, trabeculations, the LVOT, or the pulmonary valve; or missing or erroneous segmentations in one or more slices.

- Duke: 49 cases were excluded due to erroneous LV and/or RV segmentations.
- ACDC: 18 cases were excluded due to erroneous RV segmentations.
- M&Ms: 21 cases were excluded due to erroneous LV segmentations.
- M&Ms-2: 15 cases were excluded due to erroneous LV segmentations.

## D. Unique CMR input format

Similarly to what is found in the clinic, the datasets used in this study contained different image (DICOM or NIFTI) and volume (4D or 3D) formats. Therefore, the first pre-processing step was to automatically convert all scans and segmentations to a common image (NIFTI) and volume (3D) format required by the tool. A summary of the diversity of original image and volume formats is shown in Supplemental Table 6.

## E. nnU-net and the adaptive loss function

This automated segmentation framework combines dataset- and expert-driven approaches to decide the optimal framework configuration for a given imaging dataset. The former corresponds to “rule-based” parameters which depend on dataset properties, such as imaging modality or voxel size. The latter corresponds to “fixed parameters” which have been shown to work robustly across a wide range of medical imaging segmentation applications. nnU-Net performs multiple automated pre-processing steps: it crops CMR images to a region of non-zero values, it resamples all voxels to the median voxel spacing, and it performs a z-score normalisation of the intensity values. nnU-Net uses the “U-Net” architecture as a template <sup>1</sup>. However, the dataset-specific U-Net configuration - kernel size, number of pooling operations, downsampling/upsampling - is determined by the image size. At this stage, computational resources (i.e., GPU RAM) are also allocated ensuring that the batch size corresponds to less than 5% of voxels in the dataset. The model is trained for 1,000 epochs (where one epoch represents an iteration over 250 mini-batches). Weights are learned via stochastic gradient descent with Nesterov momentum ( $\mu = 0.99$ ) and an initial learning rate of 0.01 with a ‘poly’ learning rate policy  $(1 - \text{epoch}/1,000)^{0.9}$ . Deep supervision (where the contribution towards the total loss after each downsampling is halved) is used, with a combined cross-entropy and Dice loss. To tackle class imbalance, for each training image, 66.7% of patches are from random locations, while 33.3% of patches contain at least one of the foreground classes.

To tackle inconsistent image labelling (e.g., missing LVM on the ES frame) we modified nnU-Net’s loss function. The original loss function calculates the error between the predicted and manual segmentation for each label individually. This means that, when one or more labels are missing from the manual segmentation, even a perfect prediction will result in a non-zero loss. Our modification detects which labels are missing and removes these from the predicted segmentation, thus eliminating their contribution to the overall loss (e.g., if all foreground labels are missing from one patch, the loss is zero and the patch is ignored).

## F. Post-analysis quality control

Some of the criteria from the automated QA<sup>9†</sup> were also used to flag up potentially erroneous automated segmentations:

- one of its ventricular volumes being equal to zero;
- containing outliers (i.e., voxels disconnected from the main segmentation) representing more than 10% of the total number of segmented voxels - this step was first applied to a combination of all segmented labels and then to each individual label;

- any label appearing in less than 30% of segmented slices;
- presence of non-segmented slices between segmented slices for any label;
- negative or zero LV or RV stroke volume; or
- LV and RV stroke volume differences larger than 25%.

Supplemental Table 7 shows the percentage of automated segmentations that were flagged up by this post-analysis quality control (QC) for each dataset. Overall, cases were mostly flagged up due to large (>25%) stroke volume differences between the LV and the RV.



## Supplemental tables

**Supplemental Table 1 – Dice scores per scanner model**

Scanner model	LVBP		MYO		RVBP	
	ED	ES	ED	ES	ED	ES
Philips Achieva (1.5T, 3.0T) (n=297)	0.95 (0.02)	0.91 (0.05)	0.85 (0.05)	0.85 (0.05)	0.93 (0.03)	0.88 (0.05)
Siemens Aera (1.5T) (n=4936)	0.94 (0.02)	0.88 (0.05)	0.82 (0.05)	0.84 (0.04)	0.90 (0.03)	0.83 (0.06)
Siemens Avanto (1.5T) (n=272)	0.93 (0.04)	0.87 (0.07)	0.82 (0.04)	0.83 (0.05)	0.91 (0.04)	0.85 (0.08)
Siemens Biograph mMR (3.0T) (n=7)	0.95 (0.01)	0.91 (0.03)	0.86 (0.03)	N/A*	0.92 (0.02)	0.87 (0.04)
General Electric Excite (1.5T) (n=58)	0.95 (0.02)	0.89 (0.07)	0.85 (0.05)	0.87 (0.04)	0.92 (0.04)	0.88 (0.06)
General Electric HDxt (3.0T) (n=14)	0.95 (0.02)	0.92 (0.04)	0.83 (0.03)	0.86 (0.03)	0.89 (0.04)	0.86 (0.05)
Philips Ingenia (1.5T) (n=114)	0.95 (0.02)	0.92 (0.04)	0.86 (0.04)	0.84 (0.05)	0.92 (0.03)	0.88 (0.05)
Canon Orian (1.5T) (n=25)	0.94 (0.03)	0.91 (0.04)	0.83 (0.03)	0.86 (0.03)	0.92 (0.03)	0.91 (0.03)
Siemens Sola (1.5T) (n=146)	0.93 (0.03)	0.86 (0.08)	0.82 (0.04)	0.86 (0.04)	0.91 (0.03)	0.86 (0.05)
Siemens Symphony (1.5T) (n=101)	0.95 (0.02)	0.92 (0.05)	0.86 (0.05)	0.86 (0.05)	0.91 (0.06)	0.87 (0.06)
Siemens Trio (3.0T) (n=3)	0.97 (0.00)	0.92 (0.04)	0.87 (0.01)	0.86 (0.02)	0.89 (0.03)	0.82 (0.08)
Siemens Verio (3.0T) (n=47)	0.94 (0.02)	0.84 (0.09)	0.82 (0.03)	N/A*	0.91 (0.04)	0.86 (0.05)
Siemens Vida (3.0T) (n=581)	0.93 (0.02)	0.86 (0.07)	0.83 (0.03)	0.85 (0.03)	0.91 (0.04)	0.86 (0.05)

Mean (standard deviation) values for each scanner model and label (LVBP, MYO, and RVBP) in ED and ES. \*No manual segmentations contained the myocardium in ES. LVBP: LV blood pool, MYO: LV myocardium, RVBP: RV blood pool, ED: end diastole, ES: end systole.

**Supplemental Table 2 – Training and validation CMR cases**

<b>Dataset</b>	<b>Train</b>	<b>Validation, before QA<sup>gt</sup></b>	<b>Validation, after QA<sup>gt</sup></b>
NHS	2793	-	414
Duke	0	1319	1270
UKBB	0	4872	4787
ACDC	0	100	82
M&Ms	0	345	324
M&Ms-2	0	360	345

CMR cases containing segmentations that were used for training and validation (before and after QA<sup>gt</sup>). QA<sup>gt</sup>: data quality assessment of ground truth segmentations.

**Supplemental Table 3 – Dice scores per dataset (no QA<sup>gt</sup>)**

<b>Dataset</b>	<b>LVBP</b>	<b>MYO</b>	<b>RVBP</b>	<b>Average</b>
NHS	93.49 (3.76)	84.66 (4.25)	89.80 (4.43)	90.22 (5.27)
Duke	89.22 (6.80)	82.20 (4.09)	87.90 (5.92)	87.72 (6.52)
UKBB	90.79 (4.81)	82.53 (4.86)	86.64 (5.89)	86.65 (6.21)
ACDC	93.40 (5.38)	86.39 (4.69)	89.60 (6.63)	89.80 (6.31)
M&Ms	91.62 (5.72)	84.51 (4.82)	88.38 (6.90)	88.17 (6.56)
M&Ms-2	93.51 (4.02)	85.03 (5.17)	89.76 (5.47)	89.44 (6.02)

Median (interquartile range) values for each validation dataset, including values per label and their average, including cases that did not pass the QA<sup>gt</sup>. LVBP: left ventricular blood pool, MYO: left ventricular myocardium, RVBP: right ventricular blood pool, QA<sup>gt</sup>: data quality assessment of ground truth segmentations.

**Supplemental Table 4 – Absolute errors for cardiac biomarkers derived from the automated and manual segmentations (no QA<sup>gt</sup>)**

Dataset	LV				RV		
	EDV [mL]	ESV [mL]	EF [%]	LVM [g]	EDV [mL]	ESV [mL]	EF [%]
NHS	8.96 (8.04)	7.97 (6.93)	3.38 (2.83)	11.83 (9.93)	11.06 (9.43)	8.49 (7.41)	4.17 (3.39)
Duke	7.25 (6.62)	6.62 (6.24)	5.32 (4.73)	16.75 (13.70)	8.49 (8.58)	6.33 (6.17)	5.37 (4.55)
UKBB	9.36 (7.98)	9.39 (6.62)	4.67 (3.39)	7.82 (6.27)	11.51 (9.37)	10.64 (8.42)	5.31 (3.92)
ACDC	4.51 (3.39)	7.51 (6.32)	4.56 (4.31)	9.04 (8.25)	8.17 (7.54)	9.94 (10.44)	6.00 (5.28)
M&Ms	9.18 (8.78)	7.00 (6.29)	4.49 (3.93)	10.73 (10.42)	11.21 (10.24)	8.82 (10.83)	5.66 (5.22)
M&Ms-2	8.29 (7.46)	7.22 (6.29)	3.47 (3.18)	9.39 (8.53)	13.00 (13.98)	11.68 (12.20)	5.98 (4.98)

Median (interquartile range) absolute errors for cardiac biomarkers derived from the automated and manual segmentations for each validation dataset, including cases that did not pass the QA<sup>gt</sup>. QA<sup>gt</sup>: data quality assessment of ground truth segmentations.

**Supplemental Table 5 – Voxel-based segmentation statistics from external datasets.**

Dataset	Global outlier [%]	Label outliers [%]			Missing labels [%]			SV difference [%]
		LVBP	MYO	RVBP	LVBP	MYO	RVBP	
UKBB	38	34	36	49	56	67	50	200
ACDC	100	99	96	97	78	86	30	177
M&Ms	93	95	86	71	71	86	33	334
M&Ms-2	97	90	85	90	71	78	38	127

Extracted from the original manual segmentations of the ACDC, M&Ms, M&Ms-2, and UKBB datasets used to inform threshold values of the automated QA<sup>qt</sup>. The global and label outliers' values represent the percentage of originally segmented voxels that were kept after removing outliers. The missing labels' values represent the percentage of slices containing a given label when compared to the number of segmented slices. The SV difference values represent the relative difference between LV and RV stroke volumes. All shown values correspond to the most extreme CMR case from each dataset. LVBP: left ventricular blood pool, MYO: left ventricular myocardium, RVBP: right ventricular blood pool.

**Supplemental Table 6 – Original CMR image and volume formats for all datasets**

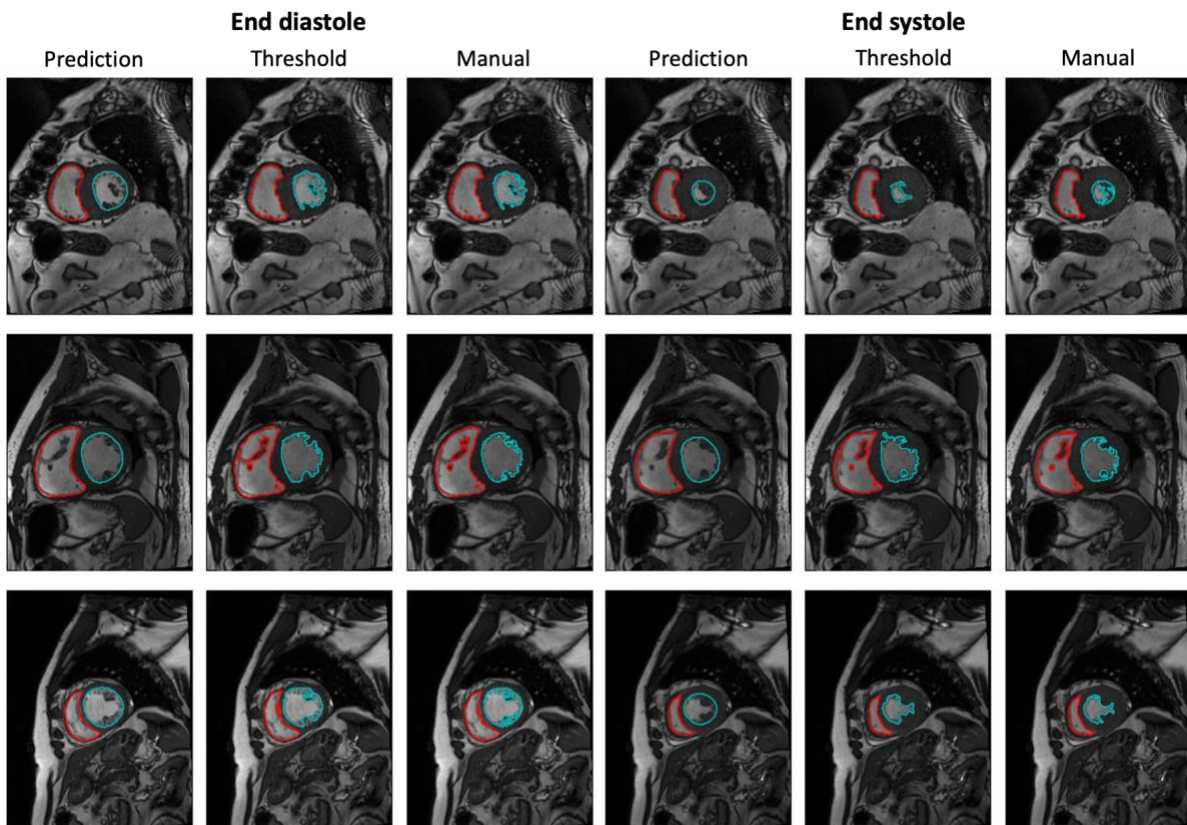
Dataset	Original image format		Original volume format	
	DICOM	NIFTI	4D	3D
NHS	x		x	
Duke	x		x	
UKBB	x		x	
ACDC		x		x
M&Ms		x	x	
M&Ms-2		x		x

**Supplemental Table 7 – Automated post-analysis quality control results**

QC	Dataset					
	NHS	Duke	UKBB	ACDC	M&Ms	M&Ms-2
Global outlier >10% [%]	0.00	0.00	0.08	0.00	0.00	0.29
LVBP outlier >10% [%]	0.00	0.00	0.04	1.22	0.00	0.58
LVM outlier >10% [%]	0.24	0.31	0.02	0.00	0.31	0.00
RVBP outlier >10% [%]	0.00	0.16	0.04	1.22	0.00	0.29
SV differences > 25% [%]	11.35	25.51	7.08	51.22	20.99	34.78
Flagged up cases [%]	11.59	25.83	7.21	52.44	21.30	35.36

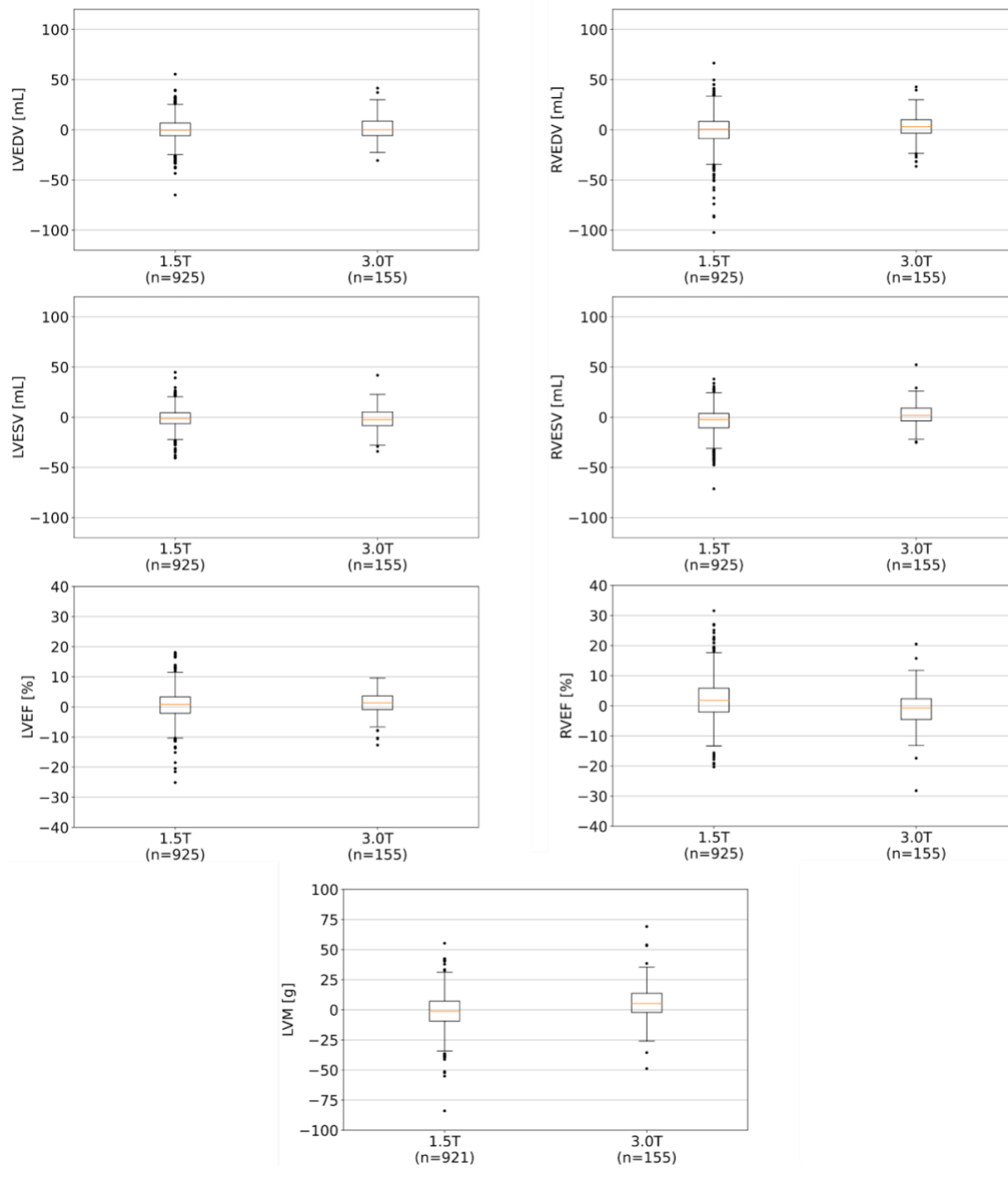
The first five rows show the percentage of cases that were flagged up for clinician review due to each of the criteria. Since some cases were flagged up after fulfilling multiple criteria, the last row indicates the percentage of cases that were flagged up at least once.

## Supplemental figures

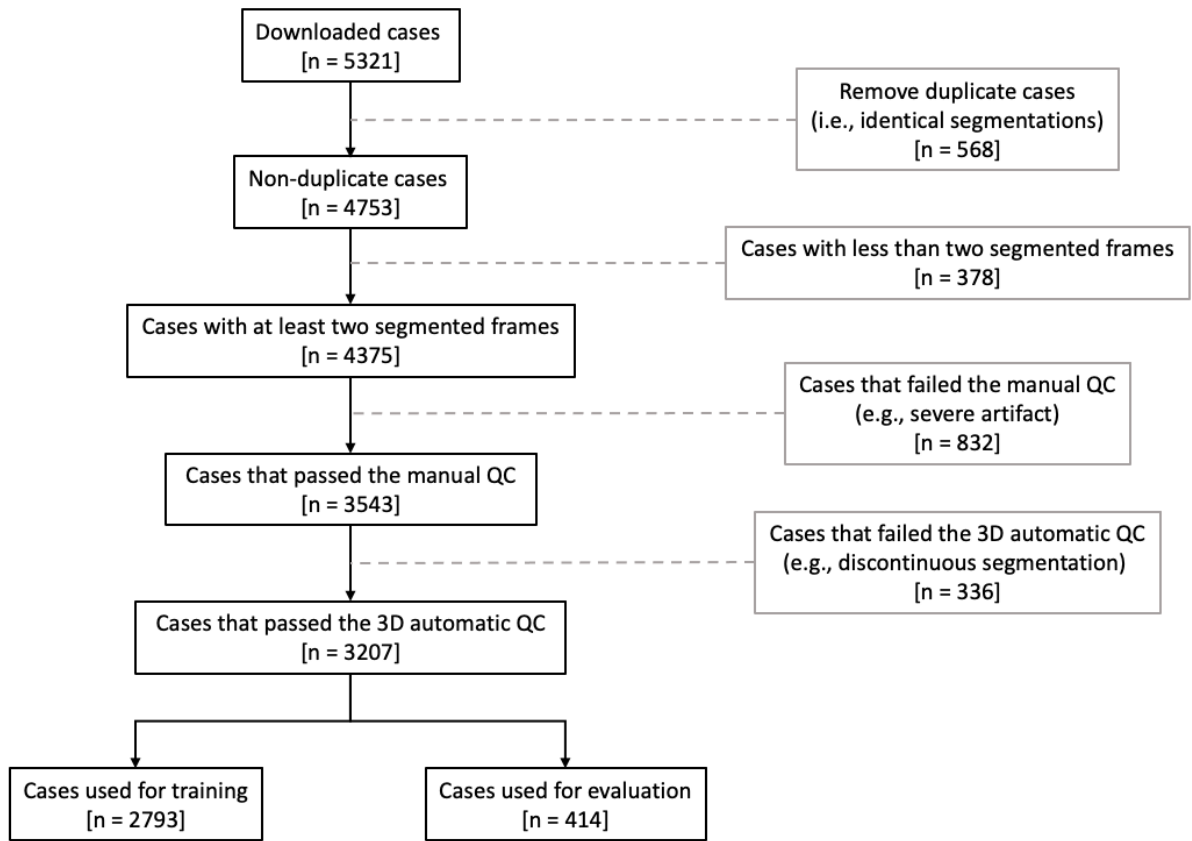


**Supplemental Figure 1 – Original vs post-processed automated segmentations for the Duke dataset:** Comparison between original and post-processed automated segmentations for the Duke dataset using Otsu’s threshold method. Each row depicts end-diastolic (left) and end-systolic (right) segmentations located in the middle of the heart for a random case.





**Supplemental Figure 2 – Box plots of cardiac biomarkers per field strength group:** Box plots of manually and automatically derived cardiac biomarkers for each magnetic field strength group. Abbreviations as in Figure 2.



**Supplemental Figure 3 – Internal (NHS) dataset curation process:** Number of NHS cases discarded during download, pre-processing, and quality assessment (QA<sup>9†</sup>).

## References

1. Ronneberger O, Fischer P, Brox T. U-Net: Convolutional Networks for Biomedical Image Segmentation. In: Navab N, Hornegger J, Wells W, Frangi A, eds. *Medical Image Computing and Computer-Assisted Intervention – MICCAI 2015. MICCAI 2015. Lecture Notes in Computer Science*. Vol 9351. Springer, Cham; 2015:234-241. doi:10.1007/978-3-319-24574-4\_28